RESEARCH BRIEF

Cellular Senescence Promotes Adverse Effects of Chemotherapy and Cancer Relapse

Marco Demaria[1,2], Monique N. O'Leary[1], Jianhui Chang[3], Lijian Shao[3], Su Liu[1], Fatouma Alimirah[1], Kristin Koenig[1], Catherine Le[1], Natalia Mitin[4], Allison M. Deal[5], Shani Alston[5], Emmeline C. Academia[1], Sumner Kilmarx[1], Alexis Valdovinos[1], Boshi Wang[2], Alain de Bruin[6,7], Brian K. Kennedy[1], Simon Melov[1], Daohong Zhou[3], Norman E. Sharpless[5], Hyman Muss[5], and Judith Campisi[1,8]

ABSTRACT

Cellular senescence suppresses cancer by irreversibly arresting cell proliferation. Senescent cells acquire a proinflammatory senescence-associated secretory phenotype. Many genotoxic chemotherapies target proliferating cells nonspecifically, often with adverse reactions. In accord with prior work, we show that several chemotherapeutic drugs induce senescence of primary murine and human cells. Using a transgenic mouse that permits tracking and eliminating senescent cells, we show that therapy-induced senescent (TIS) cells persist and contribute to local and systemic inflammation. Eliminating TIS cells reduced several short- and long-term effects of the drugs, including bone marrow suppression, cardiac dysfunction, cancer recurrence, and physical activity and strength. Consistent with our findings in mice, the risk of chemotherapy-induced fatigue was significantly greater in humans with increased expression of a senescence marker in T cells prior to chemotherapy. These findings suggest that senescent cells can cause certain chemotherapy side effects, providing a new target to reduce the toxicity of anticancer treatments.

SIGNIFICANCE: Many genotoxic chemotherapies have debilitating side effects and also induce cellular senescence in normal tissues. The senescent cells remain chronically present where they can promote local and systemic inflammation that causes or exacerbates many side effects of the chemotherapy.
Cancer Discov; 7(2); 165–76. ©2016 AACR.

INTRODUCTION

Cellular senescence is a complex stress response whereby cells irreversibly lose the capacity to proliferate, accompanied by numerous changes in gene expression (1). Many potentially oncogenic insults induce a senescence response, which is now recognized as a potent tumor-suppressive mechanism. Other senescence-inducing stimuli include radiation, genotoxic drugs, tissue injury and remodeling, and metabolic perturbations (2). Moreover, senescent cells accumulate with

[1]Buck Institute for Research on Aging, Novato, California. [2]European Research Institute for the Biology of Ageing, University Medical Center Groningen, University of Groningen, Groningen, the Netherlands. [3]Department of Pharmaceutical Sciences, University of Arkansas for Medical Sciences, Little Rock, Arkansas. [4]HealthSpan Diagnostics, Research Triangle Park, North Carolina. [5]The Lineberger Comprehensive Cancer Center and Department of Medicine, The University of North Carolina School of Medicine, Chapel Hill, North Carolina. [6]Department of Pathobiology, University of Utrecht, Utrecht, the Netherlands. [7]Department of Pediatrics, University of Groningen, University Medical Center Groningen, Groningen, the Netherlands. [8]Lawrence Berkeley National Laboratory, Life Sciences Division, Berkeley, California.

Note: Supplementary data for this article are available at Cancer Discovery Online (http://cancerdiscovery.aacrjournals.org/).

Current address for M.N. O'Leary: University of Michigan, Ann Arbor, Michigan.

Corresponding Authors: Judith Campisi, Buck Institute for Research on Aging, 8001 Redwood Boulevard, Novato, CA 94945. Phone: 415-209-2066; E-mail: jcampisi@buckinstitute.org or jcampisi@lbl.gov; and Marco Demaria, European Research Institute for the Biology of Ageing, University Medical Center Groningen, University of Groningen, Antonius Deusinglaan 1, 9713AV Groningen, the Netherlands. Phone: 31-0-6-81807878; E-mail: m.demaria@umcg.nl

doi: 10.1158/2159-8290.CD-16-0241

age in several vertebrate organisms (1), and their elimination can delay the onset of several age-associated disorders in mice (3, 4). Senescent cells most likely promote aging through the senescence-associated secretory phenotype (SASP): the increased expression and secretion of inflammatory cytokines, chemokines, growth factors, and proteases (5).

Genotoxic and cytotoxic drugs are widely used as anticancer therapies. Most such agents target proliferating cells through distinct, cell cycle–dependent mechanisms (6). Their cytotoxicity for many types of dividing cells often leads to side effects, which include immunosuppression, fatigue, anemia, nausea, diarrhea, and alopecia (7). Moreover, clinical studies of cancer survivors treated during childhood suggest that some chemotherapies cause a range of long-term side effects that resemble pathologies associated with aging, including organ dysfunction, cognitive impairment, and secondary neoplasms (8).

Many chemotherapeutic drugs alter cellular states, including the induction of senescence, in cancer cells and the tumor microenvironment (9, 10). Therapy-induced senescence (TIS) can stimulate immunosurveillance to eliminate tumor cells, but it can also be a source of chronic inflammation and drug resistance (11). Indeed, a recent study showed that treatment of patients with breast cancer with anthracycline and alkylating agents durably induces cellular senescence and a SASP in a $p16^{INK4a}$-dependent, telomere-independent fashion (12). Expression of the tumor suppressor $p16^{INK4a}$ increases with age and is a robust senescence marker in numerous mouse and human tissues (13, 14).

To more precisely assess the physiologic effects of TIS *in vivo*, we used a recently described mouse model (p16-3MR) in which $p16^{INK4a}$-positive senescent cells can be detected in living animals, isolated from tissues, and eliminated upon treatment with an otherwise benign drug (15). Using this approach, we determined the contribution of senescent cells to a variety of common short- and long-term chemotherapy toxicities. Additionally, we used a senescence marker to assess the relationship between senescent cells and chemotherapy toxicity in human patients.

RESULTS

Chemotherapy-Induced Senescence

The anthracycline antibiotic doxorubicin (Doxo) is used to treat several types of cancers in human patients. Doxo intercalates into DNA and prevents topoisomerase II from resealing the DNA double-strand break, which the enzyme creates to relieve torsional stress (16). Doxo also promotes histone eviction from chromatin, evoking a DNA-damage response and promoting changes in the epigenome and transcriptome (17). Despite reports of Doxo-induced senescence in cancer cells, little is known about how normal cells respond to Doxo.

We exposed mouse embryonic and dermal fibroblasts (MEF and MDF) to different doses of Doxo, and identified concentrations that inhibit cell proliferation (growth; Supplementary Fig. S1A and S1B). We selected 250 nmol/L, a dose at which we observed a complete growth arrest without significantly reduced viability (Supplementary Fig. S1B and not shown). MDFs treated with 250 nmol/L Doxo showed a sharp rise in senescence-associated β-galactosidase (SA-β-gal) activity and strong decline in DNA synthesis, as determined by EdU incorporation (Fig. 1A and Supplementary Fig. S1C). Senescence was further confirmed by elevated levels of mRNAs encoding $p16^{INK4a}$ and the SASP components *Il1α*, *Il6*, *Mmp3*, *Mmp9*, *Cxcl1*, *Cxcl10*, and *Ccl20* (5) using qPCR (Fig. 1B), and elevated levels of p21 and reduced levels of LaminB1 and intracellular HMGB1 proteins (5, 18, 19) using western analyses (Fig. 1C). Doxo-induced senescent cells also harbored persistent DNA damage (20), as measured by 53BP1 foci (Fig. 1D and Supplementary Fig. S1D). Importantly, Doxo induced a similar senescent phenotype, including expression of senescence markers and persistent DNA damage, in two human dermal fibroblast strains (HCA2 and BJ; Supplementary Fig. S1E–S1G and not shown).

Paclitaxel is another widely used chemotherapeutic agent that stabilizes microtubule polymers, thereby preventing their disassembly and causing an arrest of mitosis. Paclitaxel also induced senescence in mouse cells, as measured by reduced cell proliferation (Supplementary Fig. S2A), increased SA-β-gal activity (Supplementary Fig. S2B), elevated expression of $p16^{INK4a}$ and several SASP factors (*Il1α*, *Il6*, *Mmp3*, *Mmp9*, *Cxcl1*, *Cxcl10*, and *Ccl20*), as well as reduced expression of *LaminB1* (Supplementary Fig. S2C).

To determine the impact of TIS *in vivo*, we used our recently developed mouse model (p16-3MR), which contains functional domains of Renilla luciferase (LUC), monomeric red fluorescent protein (mRFP), and a truncated herpes simplex virus (HSV)-1 thymidine kinase (tTK) under control of the senescence-sensitive $p16^{INK4a}$ promoter (15). Because LUC allows the detection of 3MR-expressing cells, we followed the induction of senescent cells by bioluminescence using a range of Doxo concentrations (Fig. 1E). Acute toxicity (excessive weight loss, rough fur, and inactivity) was evident at the highest dose (25 mg/kg). We therefore used a single dose of 10 mg/kg for subsequent experiments. This dose appears to be biologically effective in that it can induce an antitumor response and toxicity (e.g., myelosuppression) but is well below the maximally tolerated doses. For comparison, human patients receive 6 to 8 biologically effective doses of Doxo at 1.25 mg/kg (~50 mg/m^2), and cumulative toxicity is observed at 12.5 mg/kg (~400 mg/m^2). Interestingly, in accord with human studies (12), this Doxo dose caused a 3-fold increase in whole-body bioluminescence (Fig. 1E and F), regardless of sex. The magnitude of the increase in bioluminescence was comparable to the increase in $p16^{INK4a}$ mRNA in different tissues, including skin, lung, and liver (Fig. 1G). Different cell types were induced to senescence by Doxo treatment, as shown in the skin where keratinocytes, endothelial cells, and, to a lesser extent, fibroblasts and smooth muscle cells were $p21^+$ by immunostaining (Supplementary Fig. S3A). Importantly, the bioluminescence and expression levels of $p16^{INK4a}$, *Il6*, and *Cxcl10* persisted for several weeks (Fig. 1H and Supplementary Fig. S3B). Similar to our data using Doxo, three other chemotherapeutic agents, paclitaxel, temozolomide (TMZ), and cisplatin, induced bioluminescence in p16-3MR mice (Supplementary Fig. S3C and S3D). Paclitaxel, TMZ, and cisplatin also elevated $p16^{INK4a}$ expression in skin (Supplementary Fig. S3E). These data indicate that cytotoxic chemotherapeutic agents with different mechanisms of action can induce senescence in primary cells in culture, and in different tissues and cell types *in vivo*.

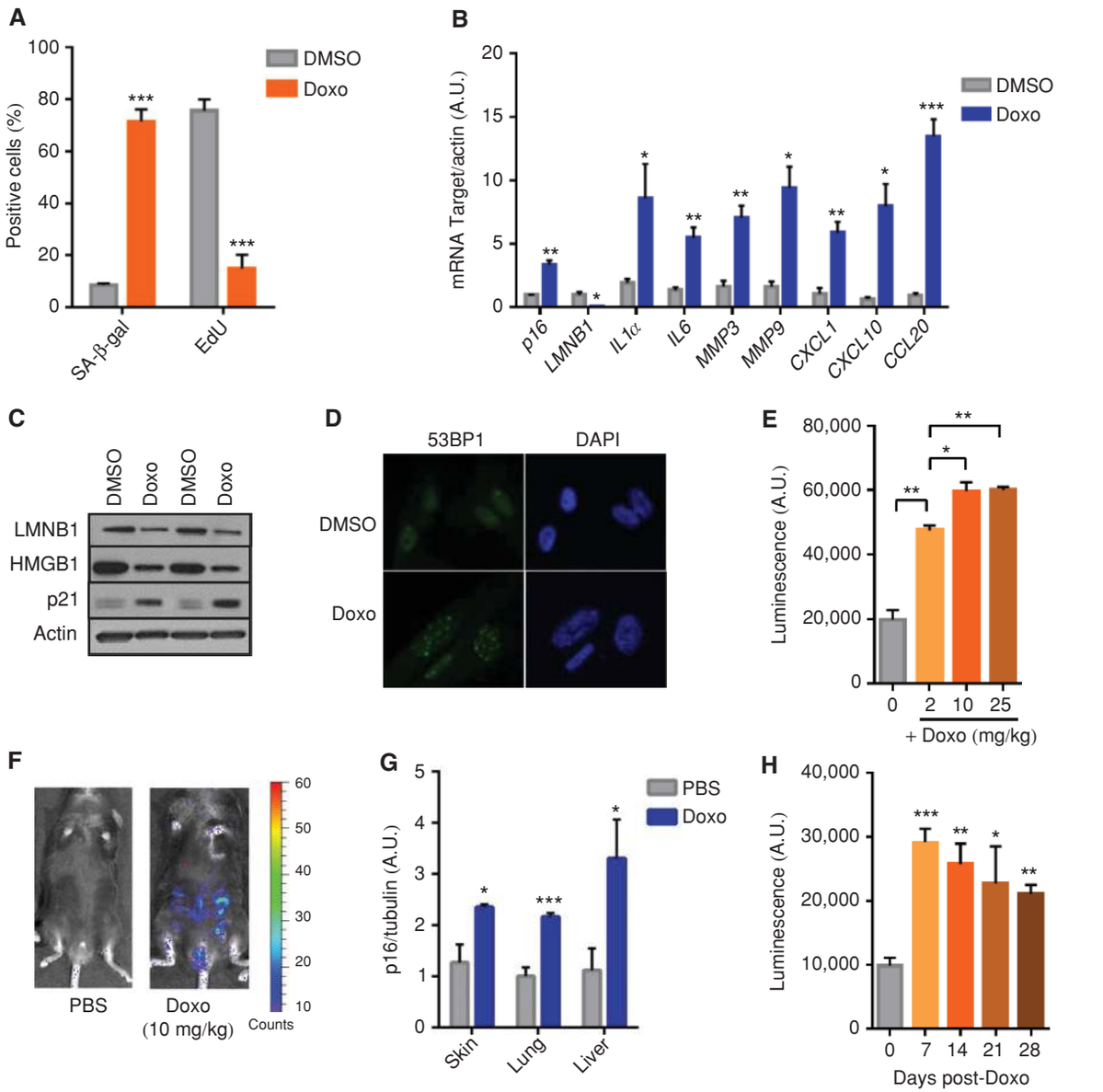

Figure 1. Therapy-induced senescence of primary cells. **A,** MDFs were treated with 250 nmol/L Doxo for 24 hours. Seven days later, cells were either fixed and stained for SA-β-gal or incubated for 24 hours with EdU then fixed and stained. Shown is the percentage of positive cells (>100 cells scored). $N = 3$ independent experiments. **B,** qRT-PCR analysis of RNA isolated from control-treated (DMSO) or Doxo-treated (250 nmol/L) MDFs. RNA was analyzed for mRNAs relative to actin (to control for cDNA quantity). $N = 3$ independent experiments. A.U., arbitrary units. **C,** Lamin B1 (LMNB1), HMGB1, and p21 protein levels were measured by immunoblotting using whole-cell extracts from control- or Doxo-treated MDFs. Actin served as a loading control. **D,** Immunofluorescence of control- or Doxo-treated cells. Blue, DAPI stained nuclei; green, 53BP1 immunostaining. **E,** p16-3MR male mice, 10 days after treatment with the indicated concentrations of Doxo (0, 2, 10, 25 mg/kg), were injected with coelentarazine and luminescence was quantified using the Xenogen Imaging system. **F,** Representative images from **E**. $N = 4$. **G,** RNA was extracted from the skin, lung, and liver of control-treated or Doxo-treated (10 mg/kg) mice, and quantified by qRT-PCR for mRNA encoding $p16^{INK4a}$. mRNA encoding tubulin was used as a control. $N = 5$. **H,** Control-treated or Doxo-treated (10 mg/kg) female mice were injected with coelentarazine, and luminescence quantified using the Xenogen Imaging system at the indicated times after Doxo treatment. $N = 4$. Data are means ± SEMs. *, $P < 0.05$; **, $P < 0.01$; ***, $P < 0.001$.

Inflammation, Bone Marrow Recovery, and Heart Function

Acute and chronic inflammatory responses are major hurdles for the beneficial outcomes of many anticancer chemotherapies (21). Indeed, high local and systemic levels of chemotherapy-induced cytokines and chemokines are associated with short-, medium-, and long-term side effects of the drugs.

Because senescent cells generated by Doxo and paclitaxel activated a SASP, which includes inflammatory factors, we investigated the impact of these cells in Doxo-treated p16-3MR mice. Senescent $p16^{INK4a}$-positive cells can be selectively eliminated from p16-3MR mice by treating the mice with

ganciclovir (GCV); the tTK moiety of 3MR phosphorylates GCV, converting it to a toxic DNA metabolite that incorporates into mitochondrial DNA and kills cells by apoptosis (15). We treated p16-3MR mice with Doxo, followed by GCV treatment 5 days later. GCV markedly reduced bioluminescence and the expression of *p16*^{INK4a} in Doxo-treated animals (Fig. 2A and B and Supplementary Fig. S4A). GCV also reduced the number of cells with DNA damage foci (Fig. 2C and Supplementary Fig. S4B). As expected, Doxo increased the expression of SASP factor genes associated with inflammation in the lungs of p16-3MR mice treated with Doxo (Fig. 2B), many (but not all) of which declined 7 days after GCV treatment (Fig. 2B). Thus, removal of senescent cells was sufficient to reduce many of the Doxo-induced inflammatory cytokines and chemokines in the tissue. Secreted factors not affected by GCV might be due to their expression by p21^{+}/p16^{INK4a-} cells, or might be independent of senescence. We also detected a significant increase in serum levels of the cytokine IL6 and chemokine CXCL1 in treatment with Doxo, which were reduced by GCV (Fig. 2D and E). As expected, Doxo-treated MEFs also secreted higher levels of IL6 and CXCL1 compared with vehicle-treated cells (Supplementary Fig. S4C and S4D).

Acute and chronic inflammatory responses often result from impairment of the immune system after chemotherapy. Indeed, bone marrow suppression is a major limiting factor for the tolerance and efficiency of these therapies. To determine whether the inflammatory indicators in Doxo-treated mice were partly due to bone marrow suppression, we determined the number and distribution of bone marrow cells (BMC) after treatment of female mice. There was a slight but not significant reduction in the total number of BMCs 2 weeks after Doxo treatment, which was rescued upon elimination of senescent cells by GCV (Supplementary Fig. S5A). We detected no differences in the percentages of Lin^{-}Sca1^{+}c-Kit^{+} (LSK) cells, hematopoietic stem cells (HSC; CD150^{+}CD48^{-}LSK cells) and hematopoietic progenitor cells (HPC; Lin^{-}Sca1^{-}c-Kit^{+} cells), suggesting the Doxo regimen we used did not affect the number or ratio of BM HSCs and HPCs (Supplementary Fig. S5B–S5D). Also, we observed no significant difference in blood cell counts, suggesting that the Doxo regimen we used induces only mild and transient myelosuppression (not shown).

We also measured HPC function by a colony formation assay. Strikingly, the number of colony-forming unit (CFU)-GEMM (granulocyte, erythrocyte, monocyte, and megakaryocyte) and CFU-GM (granulocyte and monocyte) cells was significantly reduced by Doxo treatment, but rescued upon elimination of senescent cells by GCV (Fig. 2F and G). This finding was confirmed by 2-week cobblestone area–forming cell (CAFC) assays, which measure the function of HPCs. The number of 2-week CAFCs was significantly decreased in BMCs isolated from Doxo-treated animals, but not from animals in which senescent cells were eliminated (Fig. 2H).

One major limitation to the Doxo dose that can be given to patients is cardiotoxicity, largely due to thickening of the left ventricle wall (22). Importantly, the Doxo dose used in our model was sufficient to induce cellular senescence in the heart, as measured by induction of *p16*^{INK4a} and *p21* expression (Supplementary Fig. S6A–S6C). Interestingly, the majority of cardiac senescent cells were CD31^{+} endothelial cells and, to a lesser extent, fibroblast-like cells, but not cardiomyocytes (Supplementary Fig. S6D and S6E and not shown). To evaluate heart function in mice treated with Doxo with or without the elimination of senescent cells, we used echocardiography. As expected, Doxo caused a decline in fractional shortening (contraction) and ejection fraction (blood volume pumping capacity; Fig. 2I and J). Strikingly, treatment with GCV almost completely prevented these declines (Fig. 2I and J). There was no effect of any of the treatments on heart rate (Fig. 2K). These findings indicate that senescent cells contribute to chemotherapy-induced cardiac dysfunction. Notably, the cardiac dysfunction was significantly detectable 4 weeks after Doxo treatment, but not earlier (Supplementary Fig. S6F and S6G), suggesting that the persistence of senescent cells after chemotherapy is important for the cardiotoxicity.

Thus, upon elimination of senescent cells after Doxo treatment, it was possible to reduce the burden of circulating inflammatory factors, promote the functional recovery of HPCs, and prevent cardiac dysfunction, thus limiting the drug toxicity.

Cancer Spread and Relapse

Another important side effect of chemotherapy is cancer relapse. To study the consequence of eliminating senescent cells on cancer recurrence and spread, we used the murine breast cancer cell line MMTV-PyMT, which expresses the viral oncogene Polyoma middle-T antigen. When implanted into the mammary fat pad, MMTV-PyMT cells grow *in situ* and subsequently spread to distal tissues, preferentially the lung and liver (23). We used MMTV-PyMT cells that express Firefly luciferase (fLUC), enabling us to monitor the cells in living animals by bioluminescence using a substrate distinct from that used to detect senescent cells in p16-3MR mice. Because these tumor cells do not express the p16-3MR transgene, we can distinguish the effects of chemotherapy on the tumor cells from the effects of normal cells induced to senesce by chemotherapy.

We injected fLUC-expressing MMTV-PyMT cells into mammary fat pads of p16-3MR mice. Once tumors were palpable, we treated the mice with vehicles, Doxo + PBS or Doxo + GCV. As expected, Doxo retarded or transiently arrested tumor growth, as indicated by an increase in mouse survival (Fig. 3A and Supplementary Fig. S7A). After a 1- to 2-week dormancy period, primary tumors resumed growth, with similar kinetics in the Doxo + PBS and Doxo + GCV groups (Supplementary Fig. S7A). However, mice in the Doxo + GCV group showed increased survival, which was independent of the size of the primary tumor (Fig. 3A and Supplementary Fig. S7A). Strikingly, although a majority (~80%) of mice treated with Doxo + PBS developed metastasis in the lung and liver, detectable by fLUC, many fewer (20%) mice in the Doxo + GCV group developed metastases (Fig. 3B and C). Regrowth of the primary tumors and ulcerations at the primary tumor sites prevented us from determining a full survival curve of these animals. Nonetheless, the data show that the removal of senescent cells after chemotherapy can prevent or delay cancer relapse and spread to distal tissues.

Patients diagnosed with breast cancer are most commonly treated with surgery followed by adjuvant chemotherapy or targeted therapy. To mimic this regimen in mice, we surgically removed MMTV-PyMT tumors once palpable (Supplementary Fig. S7B), then treated the animals with Doxo + PBS or Doxo + GCV. After a short latency period due to Doxo treatment,

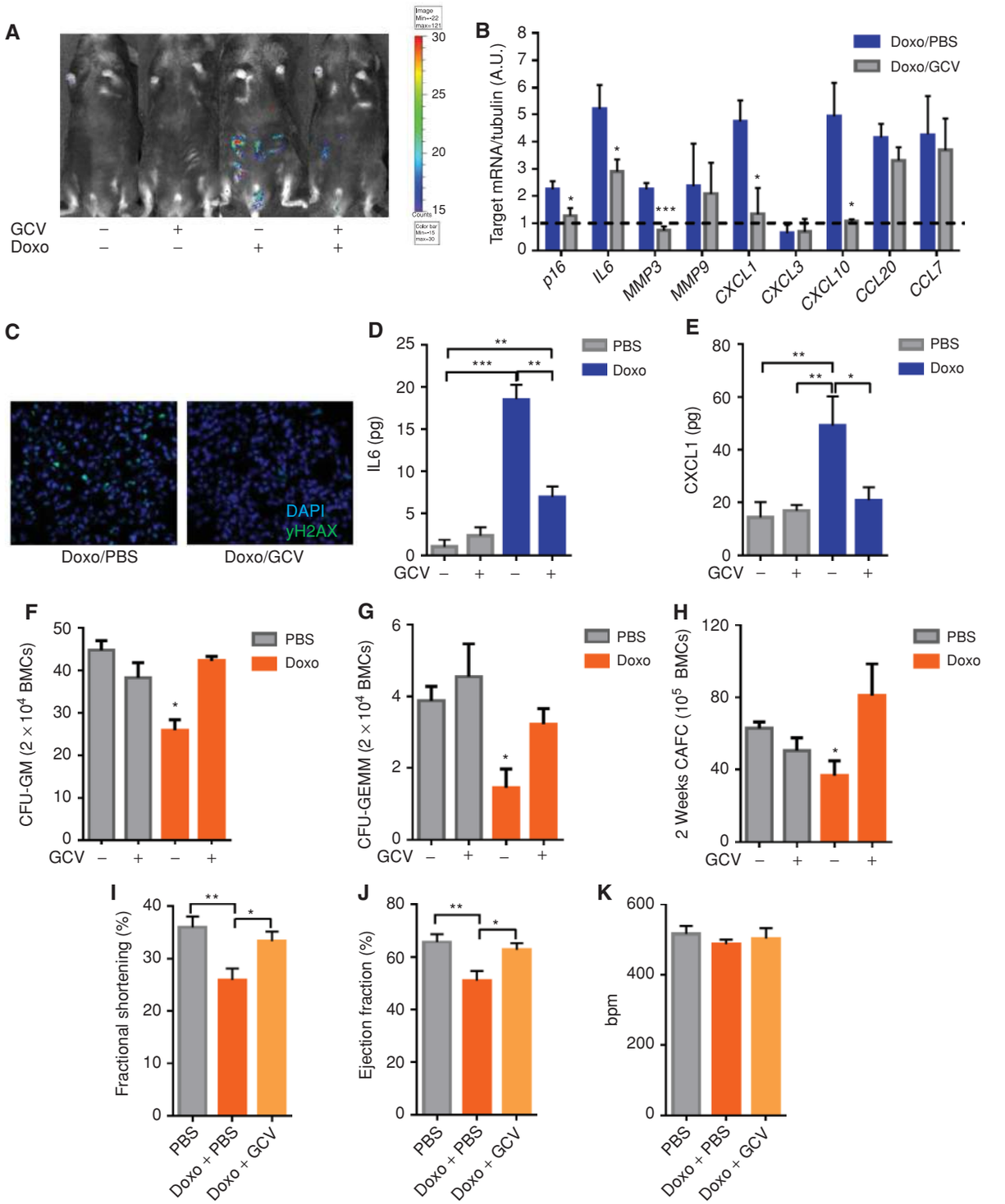

Figure 2. Senescence-associated inflammation, bone marrow suppression, and cardiac dysfunction. Control-treated or Doxo-treated (10 mg/kg) p16-3MR male mice were given vehicle (PBS) or 25 mg/kg ganciclovir (GCV) for 5 days (daily i.p. injections). **A,** Mice were injected with coelentarazine, and luminescence was monitored using the Xenogen Imaging system. **B,** qRT-PCR analysis of RNA isolated from lungs. mRNA levels were quantified relative to tubulin (control) mRNA. The dotted line indicates expression level in control mice, set at 1 for each gene. $N = 5$. A.U., arbitrary units. **C,** Lungs were fixed in paraffin and stained for γH2AX. Blue, DAPI-stained nuclei; green, γH2AX immunostaining. **D** and **E,** IL6 (**D**) and CXCL1 (**E**) levels in serum were quantified by ELISA. $N = 4$. **F–H,** Number of CFU-GM (**F**), CFU-GEMM (**G**), and 2-week CAFCs (**H**) in BMCs harvested from mice 3 days after the last PBS or GCV injection, determined by colony-forming cell and CAFC assays, respectively. $N = 3$. **I–K,** Two-dimensional transthoracic echocardiography was performed in mice 4 weeks after Doxo treatment. Graphs show fractional shortening (**I**), ejection fraction (**J**), and heartbeat (**K**) measurements. $N = 10$. bpm, beats per minute. Data are means ± SEMs. *, $P < 0.05$; **, $P < 0.01$; ***, $P < 0.001$.

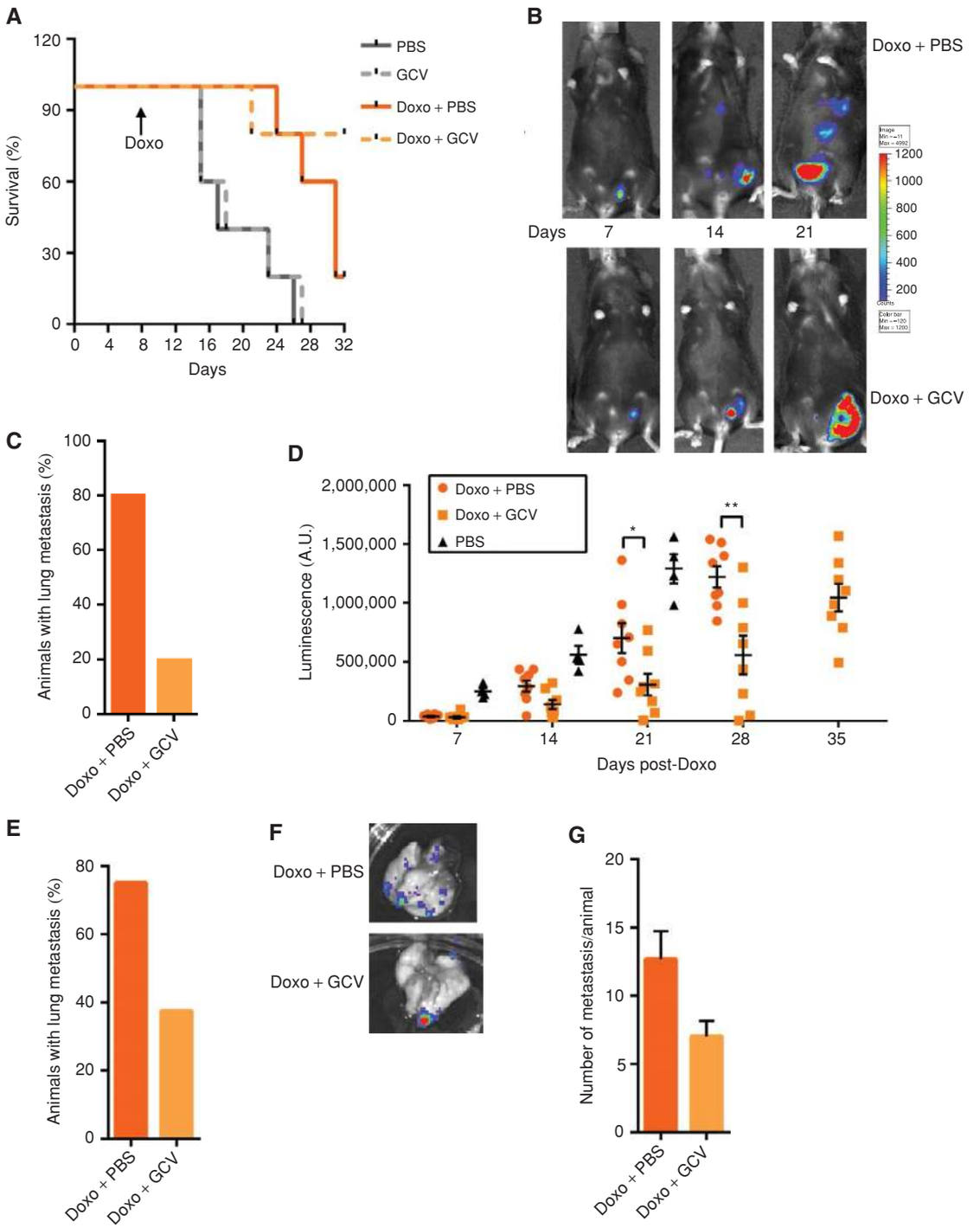

Figure 3. Senescence promotes tumor metastasis and relapse. **A–C,** fLUC-MMTV-PyMT cells (10^5) were injected into the mammary fat pad of p16-3MR female mice and treated with PBS or Doxo (10 mg/kg); 7–10 days later, the animals were injected with PBS or 25 mg/kg GCV for 5 days (daily i.p. injections). **A,** Mice were followed for survival. $N = 5$. **B,** At 7, 14, and 21 days after cancer cell injections, Doxo-treated mice were given D-Luciferin and luminescence was measured using the Xenogen Imaging system. Luminescence identified fLUC-MMTV-PyMT cells. At 21 days, the number of mice with metastasis was evaluated based on luminescence of fLUC-MMTV-PyMT cells (**C**). **D–G,** fLUC-MMTV-PyMT cells (10^5) were injected into the mammary fat pad of p16-3MR mice. Ten days later, primary tumors were surgically removed and mice were treated with Doxo (10 mg/kg), then 3 days later, with PBS or 25 mg/kg GCV for 5 days (daily i.p. injections). **D,** Mice were given D-Luciferin, and luminescence of the primary tumors was measured and quantified at the indicated time points using the Xenogen Imaging system. Luminescence identified fLUC-MMTV-PyMT cells. $N = 8$. **E,** Four weeks after Doxo treatment, metastasis was evaluated based on luminescence signals from lungs, as described in **D**. $N = 8$. **F** and **G,** Lungs were excised and luminescence was measured to quantify the number of metastasis using the Xenogen Imaging system. $N = 6$ for Doxo + PBS, $N = 3$ for Doxo + GCV. Data are means ± SEMs. *, $P < 0.05$; **, $P < 0.01$; ***, $P < 0.001$.

primary tumors recurred in all the mice (Fig. 3D). However, the kinetics of regrowth of the primary tumors depended on the type of treatment the mice received after resection (Fig. 3D and Supplementary Fig. S7C). At the time of sacrifice, tumors from the Doxo + PBS group averaged 16 mm in diameter, whereas tumors from the Doxo + GCV group averaged only 10 mm, as reflected by significant differences in the tumor bioluminescence signals (Fig. 3D, and not shown). Consistent with our finding in the previous experiment, the number of mice with metastasis was substantially lower in the Doxo + GCV group compared with the Doxo + PBS group (Fig. 3E). Moreover, mice from the Doxo + GCV group that did develop metastasis showed significantly fewer metastatic foci (Fig. 3F and G).

Although Doxo treatment likely induces senescence in the implanted tumor cells, it is important to note that the GCV treatment removes only the senescent normal host cells. Thus, these data suggest that chemotherapy can promote tumor growth and metastasis by inducing the senescence of nontumor cells.

To further prove that the removal of senescent cells, and not the GCV treatment *per se*, can delay cancer progression, we tested the effect of ABT-263, an antiapoptotic inhibitor with selective toxicity for senescent cells (24). As expected, ABT-263 eliminated Doxo-induced senescent cells from p16-3MR mice (Supplementary Fig. S8A). Moreover, mice that were injected with MMTV-PyMT cells followed by surgical removal of the tumors and treatment with a combination of Doxo and ABT-263 showed delayed tumor recurrence and metastasis, similar to the effects of GCV (Supplementary Fig. S8B and S8C).

Chemotherapy-Induced Fatigue

Asthenia (severe fatigue) is a common and important side effect of cytotoxic chemotherapy. The causes of asthenia in patients with cancer are usually multifactorial, and chemotherapy-induced fatigue can persist for long periods in patients with resolved cancer, well after the completion of chemotherapy (25). To determine whether senescent cells contribute to reduced activity after chemotherapy, we monitored Doxo-treated p16-3MR female mice with or without senescent cells for running wheel activity in metabolic cages. As expected, mice ran mainly at night, and Doxo significantly reduced the time spent running during the 12-hour nocturnal cycle (Fig. 4A). Strikingly, the elimination of senescent cells was

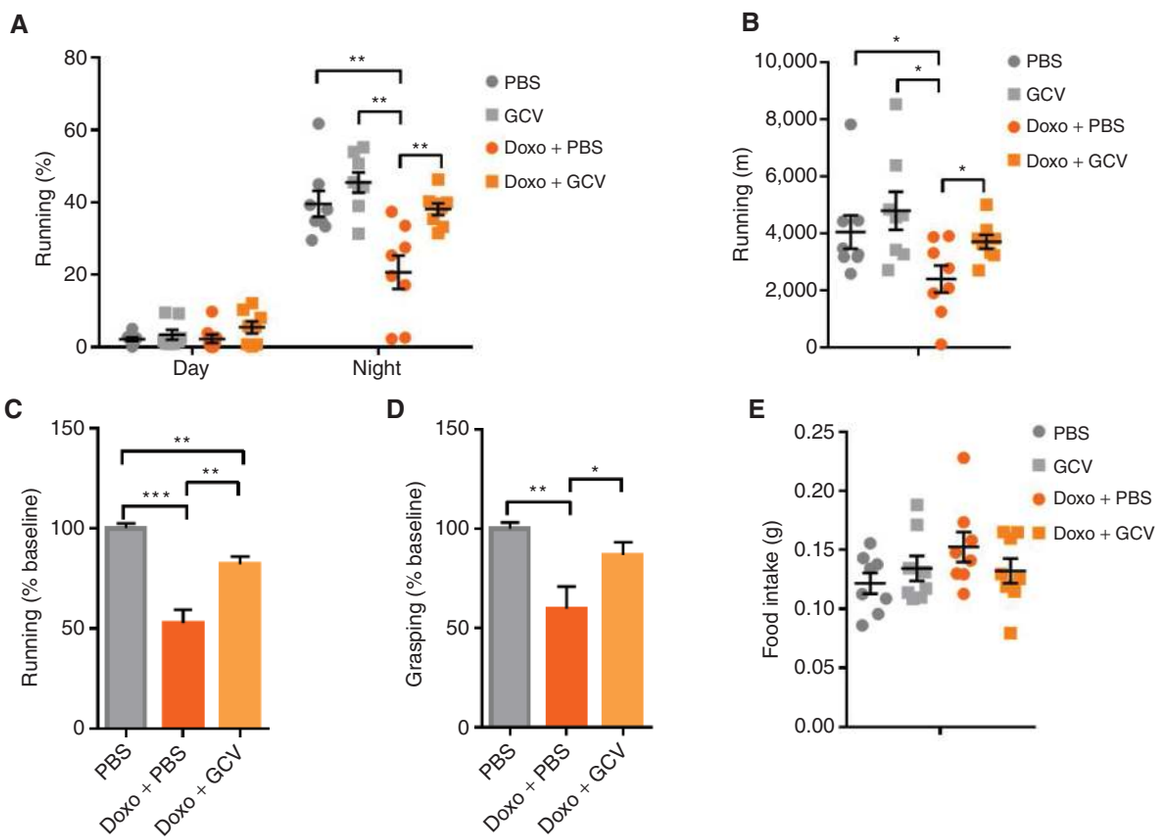

Figure 4. Effects of senescent cells on activity. Control-treated or Doxo-treated (10 mg/kg) p16-3MR female mice were treated with vehicle (PBS) or 25 mg/kg of GCV for 5 days (daily i.p. injections). **A,** Mice were single-housed in metabolic cages and monitored for 4 consecutive days. Data are the average of 4 day and night cycles and show the percentage of time spent on the running wheel. $N = 8$. **B,** Running distance in meters, calculated from the number of revolutions of the running wheel, during the nocturnal cycles (average of 4). $N = 8$. **C,** Mice were single-housed in standard cages equipped with running wheels. The number of revolutions was determined before Doxo treatment and 12 days after Doxo treatment. For each mouse, values are from an average of 3 consecutive nights. The graph shows the ratio between the post- and pretreatment running distance, expressed as a percentage. $N = 10$. **D,** Mice described in **C** were monitored for how long they were capable of grasping a reversed cage grid. For each mouse, values are an average of 5 trials. The graph shows the ratio between the post- and pretreatment grasping time, expressed as a percentage. $N = 10$. **E,** Food intake of the mice described in **A** was measured during the night cycles. Data are means ± SEMs. *, $P < 0.05$; **, $P < 0.01$; ***, $P < 0.001$.

sufficient to almost entirely rescue this decline in running activity (Fig. 4A). Because treatments with Doxo and GCV had no effect on activity and sleep during the day, we focused on the 12-hour nocturnal cycle (Fig. 4A and Supplementary Fig. S9A). During each nocturnal cycle, control mice ran an average of ~4,000 m, whereas Doxo-treated mice ran ~2,500 m; mice treated with Doxo plus GCV ran 3,800 m, which is near the activity of control mice (Fig. 4B).

To confirm the beneficial effect of eliminating senescent cells on spontaneous activity and understand the nature of this chemotherapy-induced fatigue, we monitored mice before and after treatments for running patterns and strength. Using running wheels in standard cages, we confirmed that, although Doxo/PBS-treated animals experienced a ~50% decline in running activity, the elimination of senescent cells by GCV or ABT-263 after the chemotherapy limited this reduction to ~20% (Fig. 4C and Supplementary Fig. S9B). Similarly, the decline in strength due to Doxo treatment, as measured by grasping to the cage lid, was substantially rescued by the elimination of senescent cells (Fig. 4D). Paclitaxel-treated mice experienced similar deficits in activity and strength, which were partially rescued by GCV-mediated elimination of senescent cells (Supplementary Fig. S9C and S9D). Moreover, the elimination of senescent cells from mice bearing breast cancer also substantially increased the running wheel activity of Doxo-treated mice 3 weeks after the cancer cell injections (Supplementary Fig. S9E).

Reduced spontaneous activity can be due to altered metabolism or food intake. However, from measurements made in the metabolic cages, there was no significant difference in basal metabolic rate (RQ) between control- and Doxo-treated mice, with or without senescent cells (Supplementary Fig. S10A). Moreover, food intake was comparable among the four groups, suggesting that loss of appetite or nausea was not responsible for the effects of Doxo on activity, at least for the treatment regimen used in this study (Fig. 4E). Doxo caused substantial weight loss, which showed a trend toward rescue by GCV, but the differences were not significant (Supplementary Fig. S10B).

To study the effects of senescent cells on chemotherapy-induced toxicity in humans, we used a validated marker of *in vivo* senescence, $p16^{INK4a}$ expression in peripheral blood T cells (PBTL), which we previously showed correlates with the burden of senescence in both mice and humans (12, 26–28). We asked whether this marker of organismal burden of senescent cells measured prior to therapy correlated with subsequent risk of chemotherapy-induced toxicity in a prospectively collected cohort of 89 women with breast cancer undergoing standard chemotherapy with curative intent. Patients received combinations of an anthracycline (60%), alkylating agent (89%), and/or taxane (95%), and most patients (92%) also received G-CSF (pegylated filgrastim) to minimize treatment-related neutropenia (Supplementary Table S1). We determined the correlation between prechemotherapy PBTL $p16^{INK4a}$ expression and four endpoints: fatigue, neuropathy, any hematologic toxicity, and any nonhematologic toxicity. We restricted our analyses to severe toxicity (grade III or grade IV); each of the four prespecified endpoints occurred with the expected frequency in our sample (10%–57%; Supplementary Table S2).

To test for an association between a marker of *in vivo* senescence and chemotherapy toxicity, we analyzed the data in two standard ways. First, we compared the mean $p16^{INK4a}$ expression in patients who did or did not experience a given toxicity, and tested for significance using a nonparametric test (Wilcoxon rank sum). Second, we compared the incidence of a given toxicity in patients within the highest quartile of $p16^{INK4a}$ expression versus the lowest quartile of $p16^{INK4a}$ expression and estimated relative risk using a logistic regression model that accounted for patient age and other clinical features (Supplementary Table S2). We did not observe a correlation between PBTL $p16^{INK4a}$ expression and either aggregated endpoint (all hematologic toxicities or all nonhematologic toxicities), which is not surprising given the heterogeneous nature of these complex and compound endpoints. PBTL $p16^{INK4a}$ expression measured prior to treatment was modestly higher in patients who developed severe chemotherapy-induced neuropathy (7.94 vs. 7.49; $P = 0.11$), with the incidence of severe neuropathy increased in patients within the highest quartile of $p16^{INK4a}$ expression (9% vs. 0%). The association between $p16^{INK4a}$ and neuropathy was of borderline significance, which could reflect either a chance association or weak statistical power given the small number of patients who developed grade III/IV neuropathy. There was a significant association between severe fatigue and pretreatment PBTL $p16^{INK4a}$ (7.93 vs. 7.39; $P = 0.02$). Because $p16^{INK4a}$ expression is measured on a $\log_2$ scale, this difference suggests mean $p16^{INK4a}$ expression is ~40% greater in patients who experienced fatigue. The incidence of severe fatigue in patients with the highest levels of $p16^{INK4a}$ was 44%, versus 5% in patients within the lowest quartile of $p16^{INK4a}$ expression, reflecting a ~9-fold increase in the relative risk of fatigue ($P = 0.03$). As these data were age-adjusted, this suggests an *in vivo* marker of senescence predicts toxicity independently of chronologic age. In accord with the murine findings (Fig. 4), these results suggest that the burden of senescent cells, estimated prior to therapy using PBTL $p16^{INK4a}$ expression, predicts a patient's risk of developing fatigue from cytotoxic chemotherapy.

DISCUSSION

Cellular senescence is an important tumor-suppressive mechanism that efficiently protects long-lived organisms from developing cancer at a young age (1). We and others have suggested that the SASP can serve several biological functions, either beneficial or deleterious (29). Among the deleterious effects, the accumulation and persistence of senescent cells, possibly due to decreased clearance and/or chronic induction, can disrupt tissue homeostasis and drive the onset or progression of a variety of pathologies (2). Senescent cells are generated by many types of cancer chemotherapies and can potentially fuel many aspects of cancer progression (30).

Here, we show that four commonly used chemotherapeutic drugs can induce the persistent presence of senescent cells in normal noncancerous tissues. TIS cells share several characteristics with cells induced to senesce by other stimuli, including persistent hypoproliferation, elevated expression of $p16^{INK4a}$, evidence of persistent DNA damage, and transcriptional activation of genes encoding many

SASP factors (5, 20). Because the SASP is thought to fuel the development of a variety of diseases, particularly pathologies associated with chronic inflammation (1, 2), we investigated the effects of senescent cells induced in noncancerous tissue by chemotherapy.

Many chemotherapies have short-, medium-, and long-term side effects, which often limit dosages, that require discontinuation of the treatment and/or reduce overall efficacy. Moreover, studies of cancer survivors show that one long-term effect of chemotherapy is the accelerated development of a host of age-associated diseases (8). We show that TIS cells contribute to local and systemic inflammation, as determined by increased expression of proinflammatory SASP factors in tissue and increased levels of inflammatory cytokines in sera, which is reduced after removal of senescent cells *in vivo* using p16-3MR transgenic mice. Further, the elimination of senescent cells limited or prevented the development of multiple adverse reactions to chemotherapy. In addition, weeks after chemotherapy treatment, TIS cells were important for bone marrow suppression and development of cardiac dysfunction, both limiting factors for the use of some chemotherapeutic agents, particularly the anthracyclines. The promotion of cardiac dysfunction might be due to either cardiac senescent cells, which we show are primarily endothelial cells, or senescence-induced inflammation. Senescent nontumor cells were important for cancer relapse and spread to distal tissues after chemotherapy, at least in the breast cancer model we used. Moreover, clearing senescent cells increased overall spontaneous physical activity in the presence or absence of cancer. Importantly, these murine findings were validated in a human cohort, showing that $p16^{INK4a}$ expression in peripheral T cells predicts chemotherapy-induced fatigue in human patients with breast cancer. We believe this latter finding is consistent with recent work showing that aging is the major risk factor for long-term (>2 or >5 years) fatigue after chemotherapy treatment (25).

A limitation of our study relates to the conversion of drug dosing in humans and mice. Drug pharmacokinetics and pharmacodynamics differ significantly between rodents and humans, and a potential concern of these results is that senescence induction *in vivo* results from pharmacologically unrealistic doses in mice, as opposed to those used in humans. Considering our results in pharmacodynamic rather than pharmacokinetic terms, however, we note that the murine experiments used doses of these compounds that induce a biologic effect (tumor reduction, myelosuppression, etc.) but are sublethal. This is precisely the way such agents are used in humans; that is, at doses near the maximally tolerated dose that induce tumor response as well as cytoxicity (e.g., myelosuppression). Therefore, it seems reasonable to infer that a pharmacologically active dose in either species causes the accumulation of senescent cells *in vivo*. Additionally, we showed these effects in mice with multiple compounds, suggesting that the accumulation of senescent cells in response to DNA-damaging agents appears to be a general property of cytotoxic chemotherapy administered at a biologically effective dose, and is not parochial to one of the compounds studied. Finally, we believe these results are in line with other results suggesting that cytotoxic chemotherapy induces senescence in humans (10, 12, 27, 31). In aggregate, we believe these results show that a variety of DNA-damaging agents potently and rapidly increase the *in vivo* burden of senescent cells in humans and mice, and the accumulation of such cells causes long-term toxicity for the host.

Because many cytokines, chemokines, proteases, and growth factors comprise the SASP (5), it was conceivable that senescent cells might contribute to several side effects associated with cancer treatments. The data presented here show a direct role for TIS cells in mice and a strong correlation between fatigue and senescent cells in humans. An alternative approach, then, is to develop therapies that can selectively target senescent cells (senolytics) and/or the SASP, an approach that recently showed promise (24). Indeed, the administration of a senolytic agent, ABT-263, efficiently eliminated senescent cells, improved physical activity, and reduced cancer relapse in mice treated with Doxo. Such therapeutic approaches will, of course, need to carefully consider whether there are beneficial effects of TIS, such as promoting the repair of tissues damaged by the chemotherapy or the potential of senescent cells to activate the immune response to tumor cells. Nonetheless, the pharmacologic removal of senescent cells from the tumor microenvironment might be an innovative strategy to limit toxicities of current chemotherapies, with consequent improvements in the health span and possibly life span of patients with cancer.

METHODS

Cell Preparation and Culture

Embryos 13.5 days old were dissected and cultured to produce MEFs, and fibroblasts were isolated from the dorsal skin of 3-month-old mice, as described (15). Primary mouse cells were expanded for no more than 10 doublings. Human fibroblasts (HCA2) were obtained from O. Pereira-Smith (The University of Texas Health Science Center, San Antonio). Cells were not reauthenticated by the laboratory, but regularly monitored for *Mycoplasma* contaminations (once/2 weeks). All cells were cultured in 3% oxygen for at least 4 doublings prior to use. MMTV-PyMT cells were purchased from ATCC, which validates cell lines by short tandem repeat profiling, transduced with lentiviruses expressing firefly luciferase (Perkin Elmer), and used for no more than 6 months after purchase. Doxo hydrochloride and paclitaxel (Sigma Aldrich) were dissolved in DMSO at 100 mmol/L and diluted in serum-containing medium. Cell viability was assessed using the MTS assay (Promega) according to the manufacturer's protocol.

Mice

p16-3MR mice (15) were maintained in the AAALAC-accredited Buck Institute for Research on Aging (Novato, CA) animal facility. All procedures were approved by the Institutional Animal Care and Use Committee. p16-3MR mice were bred in-house. For *in vivo* luminescence and tissue extraction, both male and female mice were used. For all the other experiments, female mice were used. For Doxo treatments, 10- to 16-week-old p16-3MR mice were injected i.p. once with 2, 10, or 25 mg/kg of Doxo hydrochloride (Sigma Aldrich) in PBS, and treated 5 days later with vehicle or GCV. GCV was administered via daily i.p. injections for 5 consecutive days at 25 mg/kg in PBS. Control mice were injected with an equal volume of PBS. For paclitaxel treatments, 10- to 16-week-old p16-3MR mice were injected 3 times i.p. (once daily for 3 consecutive days) with 10 mg/kg of paclitaxel (Sigma Aldrich) in PBS/5% DMSO, and treated 5 days later with vehicle or GCV. GCV was administered via daily i.p. injections for

5 consecutive days at 25 mg/kg in PBS. Control mice were injected with an equal volume of PBS. For temozolomide treatments, 10- to 16-week-old p16-3MR mice were injected 3 times i.p. (once daily for 3 consecutive days) with 50 mg/kg (Sigma Aldrich) in PBS/5% DMSO/0.1% Tween. For cisplatin treatments, 10- to 16-week-old p16-3MR mice were injected 3 times i.p. (once daily for 3 consecutive days) with 2.3 mg/kg (Enzo Life Sciences) in PBS/1% DMSO.

MMTV-PyMT-fLUC cells (10^5) were injected into the inguinal mammary fat pad. Surgical removal was done under total body anesthesia (isofluorane), and wounds were closed with metal stitches. Analgesia was injected subcutaneously presurgery and up to 48 hours after surgery (buprenorphine).

Real-Time PCR

Total RNA was prepared using the PureLink Micro-to-Midi total RNA Purification System (Life Technologies). RNA was reverse transcribed into cDNA using a kit (Applied Biosystems). qRT-PCR reactions were performed as described (15) using the Universal Probe Library system (Roche). Primer/probe sets for human and mouse *p16*, *LMNB1*, *IL1a*, *IL6*, *MMP3*, *MMP9*, and *CXCL1* were as previously reported (15, 32). Additionally, the following sets were used: *CXCL10* forward 5′-gctgccgtcattttctgc-3′, reverse 5′-tctcactggcccgtcatc-3′, probe #3; *CCL20* forward 5′-aactgggtgaaaagggctgt-3′, reverse 5′-gtccaattccatcccaaaaa-3′, probe #73; *CCL7* forward 5′-ttctgtgcctgctgctcata-3′, reverse 5′-ttgacatagcagcatgtggat-3′, probe 89.

Bioluminescence

For *in vivo* luminescence of Renilla Luciferase, mice were injected i.p. with 15 μg of Xenolight RediJect Coelentarazine h (Calipers/Perkin Elmer). Twenty-five minutes later, the mice were anesthetized with isofluorane and luminescence was measured with a Xenogen IVIS-200 Optical Imaging System (Caliper Life Sciences; 5-minute medium binning). For *in vivo* luminescence of Firefly Luciferase, mice were injected i.p. with 150 mg/kg of Xenolight D-Luciferin (Calipers/Perkin Elmer). Five minutes later, the mice were anesthetized with isofluorane and luminescence measured with a Xenogen IVIS-200 Optical Imaging System (Caliper Life Sciences; 3-minute medium binning).

Immunoblot Analysis

Cells were washed with warm PBS, lysed, and subjected to SDS–PAGE using 4% to 12% Bis-Tris gels; separated proteins were transferred to nitrocellulose membranes (18). Membranes were blocked and incubated for 2 hours at room temperature (LaminB1: Santa Cruz Biotechnology; HMGB1: Abcam) or overnight at 4°C (p21: Calbiochem; actin: Sigma-Aldrich) with primary antibodies. Membranes were washed and incubated with horseradish peroxidase (1:5,000; Cell Signaling)–conjugated secondary antibodies for 45 minutes at room temperature and washed again. Signals were detected by enhanced chemiluminescence.

Enzyme-Linked Immunosorbent Assays (ELISA)

ELISA kits to detect IL6 and CXCL1 were from R&D Systems and used according to the manufacturer's protocols. Conditioned media were prepared by washing cells with serum-free DMEM and incubating in serum-free DMEM for 24 hours. For Doxo-treated cells, media were collected 10 days after treatment. ELISA results were normalized to cell number. Mouse sera was isolated by centrifugation.

Immunofluorescence

Cells or optimal cutting temperature (OCT) compound–embedded lungs on glass coverslips were washed in PBS, fixed in 4% paraformaldehyde, quenched with 50 mmol/L glycine, permeabilized with 0.3% Triton X-100 in PBS, saturated with 3% goat serum (Life Technologies), and incubated with 53bp1 and γH2AX primary antibodies at room temperature (Novus Biologicals) for 1 hour, followed by incubation with Alexa fluorescein-labeled secondary antibodies (Life Technologies) for 45 minutes and mounted using Prolong Fade with Dapi (Life Technologies).

Metabolism and Activity

p16-3MR mice were individually housed for 3 days prior to being transferred to an isolated room and monitored using a Promethion system (Sable Systems) for 4 consecutive days. Alternatively, after 3 days of acclimation to single housing, mice were transferred to cages enriched with a running wheel (Columbus Instruments) and measured for 3 nights. Food intake was measured by weighing the chow every 24 hours. For grip strength, individual mice were trained for 3 trials and then grasping time measured over a subsequent 3 trials and averaged.

Collection of BMCs

The femora and tibiae were harvested from mice immediately after they were euthanized with CO_2. BMCs were flushed from the bones into Hank's Balanced Salt Solution containing 2% FCS using a 21-gauge needle and syringe. The total number of BMCs harvested from the two hind legs of each mouse was determined after red blood cells were lysed.

Analysis of the Frequencies of Hematopoietic Cell Populations by Flow Cytometry

BMCs were preincubated with biotin-conjugated anti-CD3e, anti-CD45R/B220, anti-Gr-1, anti-CD11b, and anti-TER119 antibodies and with anti-CD16/32 antibody to block the Fcγ receptors. They were then stained with streptavidin-FITC and anti-Sca1-PE-Cy7, c-Kit-APC-Cy7, CD150-APC, and CD48-Pacific blue. The frequencies of HPCs ($Lin^-Sca1^-c\text{-}Kit^+$ cells), LSK cells ($Lin^-Sca1^+c\text{-}Kit^+$ cells), and HSCs ($CD150^+CD48^-$LSK cells) were analyzed with an Aria II cell sorter. For each sample, approximately 5×10^5 to 1×10^6 BMCs were acquired and the data analyzed using BD FACSDiva 6.0 (BD Biosciences) and FlowJo software.

Colony-Forming Cell and CAFC Assays

The colony-forming cell assay was performed by culturing BM-MNCs (mononuclear cells) in MethoCult GF M3434 methylcellulose medium (Stem Cell Technologies Inc.). Colonies of CFU-GM were scored on day 7, and colonies of CFU-GEMM were scored on day 12 of the incubation, according to the manufacturer's protocol. The CAFC assay was performed as described (24).

Echocardiography

Two-dimensional transthoracic echocardiography was performed as described (29). In brief, mice were lightly anesthetized using 1.5% isoflurane mixed with 100% O_2 during the time of imaging. Echocardiography was performed prior to and following the 4-week experimental period using a LZ 550 series, 55-MHz MicroScan transducer probe and a Vevo 2100 Imaging System (VisualSonics; ref. 33). Left ventricular fractional shortening and ejection fraction were determined from the M-mode of the parasternal short-axis view. All parameters were averaged from at least 3 consecutive high-resolution cardiac cycles for analysis.

Patients

This study, LCCC 1027, was conducted with consenting adult patients undergoing treatment for breast cancer at University of North Carolina (UNC) Hospitals, and approved by the UNC Institutional Review Board and registered on clinicaltrials.gov (NCT01305954). The study was conducted in accordance with the Declaration of Helsinki. Patients over the age of 18 diagnosed with

stage I–IV breast cancer who were scheduled to start a new course of chemotherapy in the neoadjuvant, adjuvant, or metastatic setting for newly diagnosed or recurrent disease were consented to participate in the study. For this article, only neoadjuvant and adjuvant settings were analyzed. Patients with a history of clonal bone marrow disorder (e.g., acute or chronic leukemia), concurrent experimental therapy, or prior or current histone deacetylase inhibitor therapy were excluded. Patients received standard-of-care chemotherapy regimens, including the use of growth factors. Medical history and treatment information were abstracted from the medical record. Patients were also consented to undergo phlebotomy prior to the beginning of treatment for molecular analyses. Molecular analyses were performed by investigators blinded to the patient data, and investigators collecting clinical information were blinded to laboratory results until data collection was complete.

Assessment of p16 Expression

Blood (10 mL) was drawn into lavender (EDTA) tubes and used to isolate $CD3^+$ T lymphocytes. Total RNA was isolated using the RNeasy Mini Kit (Qiagen) and cDNA was prepared using ImProm-II reverse transcriptase kit (Promega). Expression of $p16^{INK4a}$ was measured by a TaqMan quantitative reverse-transcription polymerase chain reaction specific for $p16^{INK4a}$ and normalized to the *YWHAZ* housekeeping gene.

Statistical Analyses

An unpaired *t* test was used to calculate a *P* value for pairwise comparisons. *P* values on multiple comparisons were calculated using two-way ANOVA with the Bonferroni posttest. The association between $p16^{INK4a}$ and grade 3/4 toxicities was performed using one-way analysis of variance. *P* values of 0.05 or less were considered statistically significant. Wilcoxon *P* values were used because of the small size of groups. Data were analyzed by A.M. Deal using SAS version 9.2 (SAS) and STATA version 12 (StataCorp).

Disclosure of Potential Conflicts of Interest

M. Demaria has ownership interest in a patent with Unity Biotechnology. B. Kennedy reports receiving commercial research support from PDLP, has ownership interest (including patents) in L-Nutra, PDLP, and Mount Tam Biotech, and is a consultant/advisory board member for Delos. D. Zhou reports receiving a commercial research grant from, has ownership interest (including patents) in, and is a consultant/advisory board member for Unity Biotechnology. N.E. Sharpless has ownership interest (including patents) in HealthSpan Diagnostics and is a consultant/advisory board member for the same. H.B. Muss is a consultant/advisory board member for Pfizer. J. Campisi reports receiving a commercial research grant from Unity Biotechnology and has ownership interest (including patents) in the same. No potential conflicts of interest were disclosed by the other authors.

Authors' Contributions

Conception and design: M. Demaria, H. Muss, J. Campisi
Development of methodology: M. Demaria, N.E. Sharpless, J. Campisi
Acquisition of data (provided animals, acquired and managed patients, provided facilities, etc.): M. Demaria, M.N. O'Leary, J. Chang, L. Shao, S. Liu, F. Alimirah, K. Koenig, C. Le, S. Alston, E.C. Academia, B. Wang, A. de Bruin, H. Muss
Analysis and interpretation of data (e.g., statistical analysis, biostatistics, computational analysis): M. Demaria, M.N. O'Leary, J. Chang, S. Liu, F. Alimirah, A.M. Deal, S. Kilmarx, A. de Bruin, S. Melov, D. Zhou, N.E. Sharpless, H. Muss, J. Campisi
Writing, review, and/or revision of the manuscript: M. Demaria, M.N. O'Leary, N. Mitin, A.M. Deal, A. de Bruin, B.K. Kennedy, S. Melov, D. Zhou, N.E. Sharpless, H. Muss, J. Campisi
Administrative, technical, or material support (i.e., reporting or organizing data, constructing databases): S. Alston, E.C. Academia, A. Valdovinos, N.E. Sharpless, H. Muss
Study supervision: A. Valdovinos, H. Muss, J. Campisi

Acknowledgments

We thank Simone Brandenburg for helping with the titration of Doxo in cell culture. We also thank Herman Sillje for sharing the CD31 antibody.

Grant Support

This work was supported by grants from the American Italian Cancer Foundation (M. Demaria) and the NIH (AG009909, AG017242, AG041122, CA122023, and P20GM109005; J. Campisi and D. Zhou).

Received February 26, 2016; revised December 3, 2016; accepted December 13, 2016; published OnlineFirst December 15, 2016.

REFERENCES

1. Campisi J. Aging, cellular senescence, and cancer. Annu Rev Physiol 2013;75:685–705.
2. Childs BG, Durik M, Baker DJ, van Deursen JM. Cellular senescence in aging and age-related disease: from mechanisms to therapy. Nat Med 2015;21:1424–35.
3. Baker DJ, Wijshake T, Tchkonia T, LeBrasseur NK, Childs BG, van de Sluis B, et al. Clearance of p16Ink4a-positive senescent cells delays ageing-associated disorders. Nature 2011;479:232–6.
4. Baker DJ, Childs BG, Durik M, Wijers ME, Sieben CJ, Zhong J, et al. Naturally occurring p16(Ink4a)-positive cells shorten healthy lifespan. Nature 2016;530:184–9.
5. Coppe JP, Patil CK, Rodier F, Sun Y, Munoz DP, Goldstein J, et al. Senescence-associated secretory phenotypes reveal cell-nonautonomous functions of oncogenic RAS and the p53 tumor suppressor. PLoS Biol 2008;6:2853–68.
6. Dy GK, Adjei AA. Systemic cancer therapy: evolution over the last 60 years. Cancer 2008;113:1857–87.
7. Schunemann M, Anker SD, Rauchhaus M. Cancer fatigue syndrome reflects clinically non-overt heart failure: an approach towards oncocardiology. Nat Clin Pract Oncol 2008;5:632–3.
8. Hudson MM, Ness KK, Gurney JG, Mulrooney DA, Chemaitilly W, Krull KR, et al. Clinical ascertainment of health outcomes among adults treated for childhood cancer. JAMA 2013;309:2371–81.
9. Schmitt CA. Senescence, apoptosis and therapy–cutting the lifelines of cancer. Nat Rev Cancer 2003;3:286–95.
10. Sun Y, Campisi J, Higano C, Beer TM, Porter P, Coleman I, et al. Treatment-induced damage to the tumor microenvironment promotes prostate cancer therapy resistance through WNT16B. Nat Med 2012;18:1359–68.
11. Ewald JA, Desotelle JA, Wilding G, Jarrard DF. Therapy-induced senescence in cancer. J Natl Cancer Inst 2010;102:1536–46.
12. Sanoff HK, Deal AM, Krishnamurthy J, Torrice C, Dillon P, Sorrentino J, et al. Effect of cytotoxic chemotherapy on markers of molecular age in patients with breast cancer. J Natl Cancer Inst 2014;106:dju057.
13. Ressler S, Bartkova J, Niederegger H, Bartek J, Scharffetter-Kochanek K, Jansen-Durr P, et al. p16INK4A is a robust in vivo biomarker of cellular aging in human skin. Aging Cell 2006;5:379–89.
14. Krishnamurthy J, Torrice C, Ramsey MR, Kovalev GI, Al-Regaiey K, Su L, et al. Ink4a/Arf expression is a biomarker of aging. J Clin Invest 2004;114:1299–307.
15. Demaria M, Ohtani N, Youssef SA, Rodier F, Toussaint W, Mitchell JR, et al. An essential role for senescent cells in optimal wound healing through secretion of PDGF-AA. Dev Cell 2014;31:722–33.
16. Pommier Y, Leo E, Zhang H, Marchand C. DNA topoisomerases and their poisoning by anticancer and antibacterial drugs. Chem Biol 2010;17:421–33.
17. Pang B, Qiao X, Janssen L, Velds A, Groothuis T, Kerkhoven R, et al. Drug-induced histone eviction from open chromatin contributes to

the chemotherapeutic effects of doxorubicin. Nat Commun 2013; 4:1908.
18. Freund A, Laberge RM, Demaria M, Campisi J. Lamin B1 loss is a senescence-associated biomarker. Mol Biol Cell 2012;23:2066–75.
19. Davalos AR, Kawahara M, Malhotra GK, Schaum N, Huang J, Ved U, et al. p53-dependent release of Alarmin HMGB1 is a central mediator of senescent phenotypes. J Cell Biol 2013;201:613–29.
20. Rodier F, Coppe JP, Patil CK, Hoeijmakers WA, Munoz DP, Raza SR, et al. Persistent DNA damage signalling triggers senescence-associated inflammatory cytokine secretion. Nat Cell Biol 2009;11:973–9.
21. van der Most RG, Currie AJ, Robinson BW, Lake RA. Decoding dangerous death: how cytotoxic chemotherapy invokes inflammation, immunity or nothing at all. Cell Death Differ 2008;15:13–20.
22. Singal PK, Iliskovic N. Doxorubicin-induced cardiomyopathy. N Engl J Med 1998;339:900–5.
23. Fantozzi A, Christofori G. Mouse models of breast cancer metastasis. Breast Cancer Res 2006;8:212.
24. Chang J, Wang Y, Shao L, Laberge RM, Demaria M, Campisi J, et al. Clearance of senescent cells by ABT263 rejuvenates aged hematopoietic stem cells in mice. Nat Med 2016;22:78–83.
25. Kreissl S, Mueller H, Goergen H, Mayer A, Brillant C, Behringer K, et al. Cancer-related fatigue in patients with and survivors of Hodgkin's lymphoma: a longitudinal study of the German Hodgkin Study Group. Lancet Oncol 2016;17:1453–62.
26. Liu Y, Sanoff HK, Cho H, Burd CE, Torrice C, Ibrahim JG, et al. Expression of p16(INK4a) in peripheral blood T-cells is a biomarker of human aging. Aging Cell 2009;8:439–48.
27. Wood WA, Krishnamurthy J, Mitin N, Torrice C, Parker JS, Snavely AC, et al. Chemotherapy and Stem Cell Transplantation Increase p16INK4a Expression, a Biomarker of T-cell Aging. EBioMedicine 2016;11:227–38.
28. Burd CE, Sorrentino JA, Clark KS, Darr DB, Krishnamurthy J, Deal AM, et al. Monitoring tumorigenesis and senescence in vivo with a p16(INK4a)-luciferase model. Cell 2013;152:340–51.
29. Demaria M, Desprez PY, Campisi J, Velarde MC. Cell autonomous and non-autonomous effects of senescent cells in the skin. J Invest Dermatol 2015;135:1722–6.
30. Dorr JR, Yu Y, Milanovic M, Beuster G, Zasada C, Dabritz JH, et al. Synthetic lethal metabolic targeting of cellular senescence in cancer therapy. Nature 2013;501:421–5.
31. Beeharry N, Broccoli D. Telomere dynamics in response to chemotherapy. Curr Mol Med 2005;5:187–96.
32. Laberge RM, Sun Y, Orjalo AV, Patil CK, Freund A, Zhou L, et al. MTOR regulates the pro-tumorigenic senescence-associated secretory phenotype by promoting IL1A translation. Nat Cell Biol 2015;17: 1049–61.
33. Flynn JM, O'Leary MN, Zambataro CA, Academia EC, Presley MP, Garrett BJ, et al. Late-life rapamycin treatment reverses age-related heart dysfunction. Aging Cell 2013;12:851–62.